Retinal Disease Classification from OCT Images Using Deep Learning Algorithms

Jongwoo Kim
Lister Hill National Center for Biomedical Communications
National Library of Medicine, National Institutes of Health
Bethesda, USA
jongkim@mail.nih.gov

Loc Tran
Lister Hill National Center for Biomedical Communications
National Library of Medicine, National Institutes of Health
Bethesda, USA
lotran@mail.nih.gov

Abstract—Optical Coherence Tomography (OCT) is a non-invasive test that takes cross-section pictures of the retina layer of the eye and allows ophthalmologists to diagnose based on the retina's layers. Therefore, it is an important modality for the detection and quantification of retinal diseases and retinal abnormalities. Since OCT provides several images for each patient, it is ~~a~~ time consuming work for ophthalmologists to analyze the images. This paper proposes deep learning models that categorize patients' OCT images into four categories such as Choroidal neovascularization (CNV), Diabetic macular edema (DME), Drusen, and Normal. Two different models are proposed. One is using three binary Convolutional Neural Network (CNN) classifiers and the other is using four binary CNN classifiers. Several CNNs, such as VGG16, VGG19, ResNet50, ResNet152, DenseNet121, and InceptionV3, are adapted as feature extractors to develop the binary classifiers. Among them, the proposed model using VGG16 for CNV vs. Other classes, VGG16 for DME vs. other classes, VGG19 for Drusen vs. Other classes, and InceptionV3 for Normal vs. other classes shows the best performance with 0.987 accuracy, 0.987 sensitivity, and 0.996 specificity. The binary classifier for Normal class has 0.999 accuracy. These results show their potential to work as a second reader for ophthalmologists.

Keywords— Optical Coherence Tomography (OCT), Retinal Disease, Deep Learning, Convolutional Neural Networks (CNN), Fully Convolutional Neural Networks (FCN)

I. INTRODUCTION

Optical coherence tomography (OCT) is a non-invasive imaging technique that generates cross-sectional images of the retina layer of the eye. It uses light waves in the near-infrared spectral range which has a penetration depth of several hundred microns in the retina layer. Therefore, it is an important modality for ophthalmologist to detect/quantify retinal diseases and retinal abnormalities and to provide treatment guidance for glaucoma, age-related macular degeneration (AMD), diabetic retinopathy, choroidal neovascularization (CNV), and Diabetic macular edema (DME) [1, 2]. AMD has two types: Dry AMD and Wet AMD. Dry AMD patients have Drusen, and most Wet AMD patients have Choroidal Neovascularization (CNV) and associated manifestations in their retinas [3, 4, 5]. CNV is the growth of abnormal blood vessels in the choroid layer of retina [6]. DME is an accumulation of fluid in the macula part of the retina due to blood vessel leakage. About 25% of Diabetic Retinopathy patients develop to DME [7, 8]. However, it is ~~a~~ time-consuming work for ophthalmologists to analyze the OCT images since OCT provides several images for each patient.

Deep learning algorithms have been adapted for the classification of OCT images recently. DenseNet201 [9] (and the other ten CNNs) are used for the classification of OCT images into the four classes [10]. Inception V3 [11] is adapted to classify OCT images into four classes such as CNV, DME, Drusen, and Normal [12]. Ensemble learning based on ResNet152 [13] are used to classify OCT images into the four classes [14]. Modified ResNet50 [13] and ensemble learning are used to classify the images into the four classes [15]. Image normalization and VGG16 [16] are used to train OCT images for the classification of the four classes [17]. Four binary classifiers based on ResNet101 [13] are trained to classify cystoid macular edema, macular hole, epiretinal membrane, and serous macular detachment from OCT images [18]. In training CNNs, pre-trained weights, provided by the ImageNet [19], are used as initial weights or feature extractors in most of above studies since the weights are obtained from training large image datasets.

There are two types of deep learning (DL) models used in the above studies. One is using multi-class classifiers and the other is using multiple binary classifiers. To resolve multi-class classification cases, the DL model using a multi-class classifier (DLM) is more convenient than the DL model using binary classifiers (DLB) since DLM needs to train only one classifier. The DLB needs to train multiple classifiers for each class. However, there is an advantage in using the DLB when we try to update/improve the model to classify one or more new classes in the same dataset after developing the model. The DLB only needs to train new binary classifiers for new classes. However, the DLM needs to train the model again from the beginning. The DLB has more extensibility than the DLM. Multiple binary classifiers also show better performance than one multi-class classifier in image segmentation case [20].

Therefore, this paper proposes two DL models that classify patients' OCT images into four categories such as CNV, DME, Drusen, and Normal. Four binary CNN classifiers (for CNV, DME, Drusen, and Normal classes) and three binary CNN classifiers (for CNV vs. DME, Drusen vs. Normal, and CNV-DME vs. Drusen-Normal) are used to design the architectures of

the proposed models. A preprocessing algorithm is adapted to remove noises and crop retina layers from the images.

The remainder of this paper is organized as follows. Section II describes the dataset and our methods to classify OCT images in detail. We discuss experimental results in Section III, and conclude in Section IV.

II. Methods

A. OCT Image and Image Dataset

An optical coherence tomography (OCT) image dataset is used in this experiment [12]. It is a publicly available and was collected from five institutes from 2013 to 2017. The dataset is composed of 108,309 training images and 1,000 test images. It contains four classes as shown in Table 1; CNV class has 37,205 images, DME class has 11,348 images, Drusen class has 8,616 and Normal class has 51,140. In the test dataset, each class has 250 images.

TABLE I. Training and Testing Datasets used For the Experiment

Class	Train	Test
CNV	37,205	250
DME	11,348	250
Drusen	8616	250
Normal	51,140	250

Fig. 1 shows an OCT image in Normal class. Since OCT images are grey level images, image intensity is very important feature to classify the images into the four classes. There are three boundaries of interest in the image as shown in Fig. 1. They are Inner limiting Membrane (ILM) in yellow, Retinal Pigment Epithelium (RPE) in red, and Chorio-Scleral Interface (CSI) in green. Among the boundaries, RPE is one of the most important layers for the classification. It is the brightest layer in the middle. In the case of CNV, it consists of an abnormal growth of vessels from the choroidal vasculature to the neurosensory retina through the Bruch's membrane. Therefore, there are variation in below or above RPE or intra-retinal area (showing macular fluid in black color, bumpy RPE layer, and poor defined boundaries). In the case of DME, there is intra-retinal fluids between ILM and RPE. The fluids are shown in dark color. In the case of Drusen, RPE layer has bumpy shape instead of a flat shape.

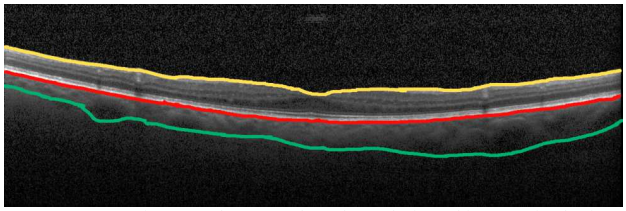

Figure 1. An OCT image. There are three boundaries of interest in the images such as Inner limiting Membrane (ILM) in yellow, Retinal Pigment Epithelium (RPE) in red, and Chorio-Scleral Interface (CSI) in green.

B. Image Normalization

The images in the dataset have different sizes and qualities, and most images have black and white noise as shown in Fig. 2. The first row is for CNV class, the second row is for DME class, the third row is for Drusen class, and the fourth row is for Normal class. In the case of the images in the first column, all images have a square shape. However, the images in the second column do not have a square shape and have white background. The images in the third column have black and white noises in the background. In addition, zoom rates are different to each other. The images in the second column have less zoom ratio compared with images in the first and third columns. The image in the first row third column has more zoom ratio than other images.

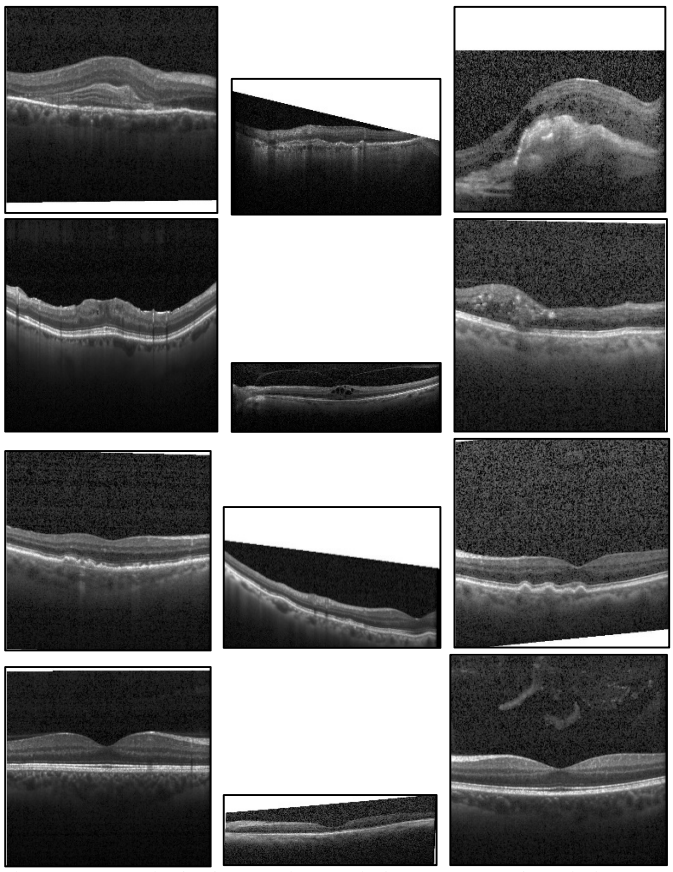

Figure 2. Images in the dataset. First row is for CNV, second row is for DME, third row is for Drusen, and fourth row is for Normal.

As we discuss in Section II.A, white pixels are very important features in OCT images for classification. However, several images are contaminated by white background noises and black and white noises. If the majority of the images in a class have white background noises, CNNs can misuse the noises as strong features for the class during the training process. This dataset has 108,309 images; therefore, it is hard to check the status of all images and trim mislabeled images before training.

Therefore, the following procedure is adapted to normalize the images in the dataset as shown in Fig. 3 [14]. This procedure allows CNN classifiers to easily estimate features from images for training. First, read an input image. Second, replace the white colored background with a black color background, and make a square image. Third, estimate retina layers using a Fully Convolutional Networks (FCN) having a U-Net architecture

[21]. Fourth, remove the black and white noise using the FCN result. Fifth, adjust the rotated retina layer by using a histogram estimated by projecting an image into vertical axis. Sixth, crop only retina layer from the image. Inputs of the FCN are 224×224×3 images and outputs are 224×224×1 grey images. 1,000 images (250 images from each class) are used to train the FCN. Python with Tensorflow Keras [22, 23] is used for the implementation of the FCN.

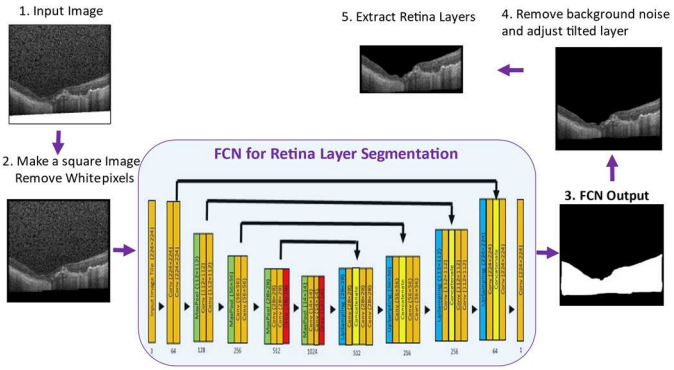

Figure 3. Workflow of image normalization using the FCN with a U-Net architecture.

C. *Proposed CNN for Binary Classification*

Fig. 4 shows the architecture of the proposed binary CNN classifier. Six different CNN models, such as VGG16, VGG19, ResNet50, ResNet152, DenseNet201, and InceptionV3, are used as feature extractors for the classification. Following the CNN feature extractor, a global average pooling layer, dense layer, dropout layer, dense layer, dropout layer, and output softmax layer are added in this sequence. The size of the dense layers is 1×1,024, and dropout ratio = 0.5 is used for the two dropout layers to resolve overfitting issues. We use pre-trained weights of the ImageNet [19] as initial weights of the feature extractors and train all layers in the architecture including the layers in the CNN feature extractor.

D. *Proposed Deep Learning Models*

We propose two deep learning models based on the proposed binary classifier (Fig. 4).

The first model (Model 1) uses three binary CNN classifiers as shown in Fig 5. Classifier 1 is for the (CNV and DME) vs. (Drusen and Normal) classes, Classifier 2 is for CNV vs. DME class, and Classifier 3 is for Drusen vs. Normal class. CNV and DME are more serious conditions than Drusen and Normal. Therefore, we first categorize the images into the two classes, (CNV and DME) vs. (Drusen and Normal), using Classifier 1. Then we label the class of each image using Classifier 2 and 3.

The second model (Model 2) uses four binary CNN classifiers as shown in Fig 6. Classifier 1 is for the CNV class, Classifier 2 is for the DME class, Classifier 3 is for the Drusen class, and Classifier 4 is for the Normal class. We call Classifier 1 as Classifier-CNV, Classifier 2 as Classifier-DME, Classifier 3 as Classifier-Drusen, and Classifier 4 as Classifier-Normal from now on. Classifier-CNV classifies input images into two classes (CNV class vs. Other class). Therefore, the other class includes images that belong to DME, Drusen, and Normal classes. Similar rules are applied to the other classifiers. Classifier-DME is for DME class vs. Other class. Classifier-Drusen is for Drusen class vs. Other class. Classifier-Normal is for Normal class vs. Other class.

Since all classifiers are binary classifiers, outputs of the classifiers have a two dimensional format (1 × 2). The outputs are converted to a four dimensional format. (1 × 4). In the case of Model 1, when Classifier 1, 2, and 3 have outputs [(CNV and DME), (Drusen and Normal)] = [0.8, 0.2], [CNV, DME] = [0.8, 0.2], and [Drusen, Normal] = [0.6, 0.4], the multiplication results of Classifier 1 and 2, and Classifier 1 and 3 have [CNV, DME] = 0.8 × [0.8, 0.2] = [0.64, 0.16] and [Drusen, Normal] = 0.2 × [0.6, 0.4] = [0.12, 0.08]. Therefore, the final result becomes [CNV, DME, Drusen, Normal] = [0.64, 0.16, 0.12, 0.08]. In the case of Model 2, when a Classifier-CNV output is [CNV, Other] = [0.8, 0.2], the output is converted to [CNV, DME, Drusen, Normal] = [0.8, 0.2, 0.2, 0.2]. The similar rules are applied to the outputs of the remaining three classifiers. Afterwards, all four (four-dimensional) outputs are multiplied to estimate the final probabilities of each class. For example, to estimate final probability of CNV for an input image, four CNV probabilities from the four classifiers are multiplied. Similar rules are applied to estimate probabilities of DME, Drusen, and Normal.

We also trained the weights for each classifier to combine the results of all classifiers in Model 1 and 2. However, we did not find any performance differences compared with our methods based on probability theory.

Python with Tensorflow Keras [22, 23] is used to implement the proposed deep learning model.

III. Experimental Results and Discussion

We generate a training set by sampling 8,616 images from each class. The training dataset has an unbalanced number of images in between classes. Class weight is commonly used in training process to resolve the unbalanced class issue. However, this does not improve the classification accuracy in our case. Therefore, we collect 8,616 images from each class using a random sampling method. In addition, we normalize OCT images by cropping the retina layers using the FCN as shown in Fig. 3. Therefore, we do not use image augmentation technique to increase the training data.

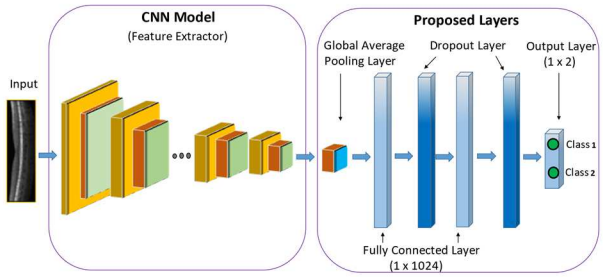

Figure 4. Architecture of the proposed binary CNN classifier.

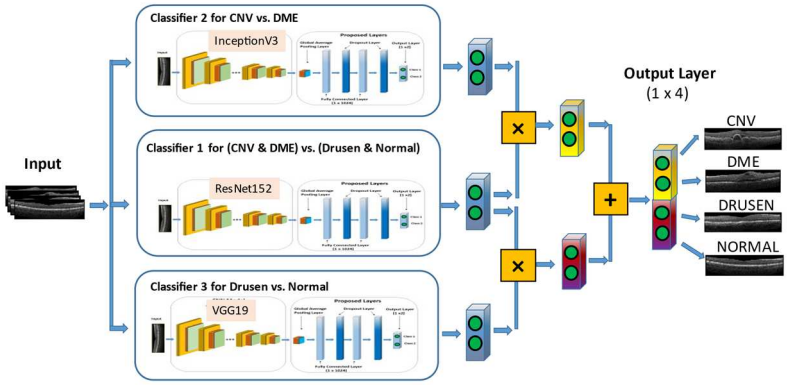

Figure 5. Architecture of the proposed deep learning model 1 (Model 1).

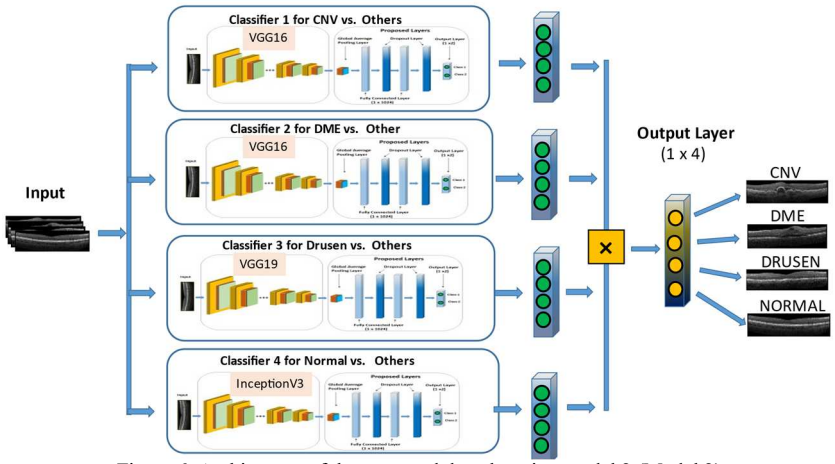

Figure 6. Architecture of the proposed deep learning model 2 (Model 2).

To train the classifiers, we use stochastic gradient descent (SGD) with learning rate = 0.001, decay=1e-6, momentum = 0.9, nesterov momentum = True, and epochs = 50 and 100. The hardware configuration used for this experiment is 2 × Intel Xeon Gold 5218 processors 2.3 GHz, 64 hyper-thread processors, 8 × RTX 2080 Ti, and Red Hat Enterprise Linux 7.

Original dataset (Table 1) contains the test dataset with 250 images for each class. Several deep learning algorithms use this test dataset for their evaluation. Therefore, we use the same original test dataset to evaluate our performance with others.

Table II shows the comparison of the two types of OCT images: original and normalized. We train four binary classifiers using the two types of images. The classifiers using the normalized images always show better performance. We assume the normalized images make the CNN classifiers focus on features in the images more accurately during training time. This result proves the benefit of using the proposed image normalization process.

Table III shows our classification results of the proposed Model 1. We train the three binary classifiers using the six different CNN feature extractors. Among them, the model using three InceptionV3 classifiers shows the best performance with 0.9770 accuracy. When we use the best three classifiers (ResNet152 for Classifier 1, InceptionV3 for Classifier 2, and VGG19 for Classifier 3), the proposed Model 1 shows the best performance with 0.9810 accuracy.

Table IV shows our classification results of the proposed Model 2. Among them, the model using four VGG19 classifiers shows the best performance with 0.9780 accuracy. When we use the best four classifiers (VGG16 for Classifier-CNV and Classifier-DME, VGG19 for Classifier-Drusen, and InceptionV3 for Classifier-Normal), the proposed Model 2 shows the best performance with 0.9870 accuracy. The Model 2 shows a better performance than the Model 1.

TABLE II. COMPARISON OF THE TWO OCT IMAGE TYPES USING THE PROPOSED FOUR BINARY CLASSIFIERS USED IN THE PROPOSED MODEL 2

Image Type	Classifier	CNNs	Acc.
Original OCT Images	CNV	VGG16	0.967
	DME	VGG16	0.993
	Drusen	VGG19	0.976
	Normal	InceptionV3	0.995
Normalized OCT Images	CNV	VGG16	0.976
	DME	VGG16	0.997
	Drusen	VGG19	0.981
	Normal	InceptionV3	0.999

Fig. 7 shows ROC curves of the four binary CNN classifiers used in the proposed model (Model 2) in the last row in Table IV. The curve of each classifier uses different color. Green is for Classifier-CNV, blue is for Classifier-DME, red is for Classifier-Drusen, and yellow is for Classifier-Normal. The left figure shows ROC curves and the right figure shows the curves zoomed in the top left corner of the ROC curves. Among the classifiers, Classifier-Normal shows the best performance. Fig. 8 shows ROC curves of the proposed Model 2. The left figure shows a ROC curve and the right figure shows the curve zoomed in the top left corner of the ROC curve.

Fig. 9 shows the confusion matrices of the binary classifiers used in the proposed methods. Fig. 9(a) shows the confusion matrices of the best three classifiers for Model 1. Among the classifiers, Classifier 3 for Drusen vs. Normal (right) shows the best performance. One Drusen and three Normal class images are misclassified. Classifier 1 for CNV-DME vs. Drusen-Normal (left) shows the largest error ratio. Two CNV-DME and 25 Drusen-Normal class images are misclassified. Fig. 9(b) shows the confusion matrices of the best four classifiers for Model 2. Among the classifiers, Classifier-Normal shows the best performance. It misclassifies only one Normal image as Other. Classifier-CNV shows the largest errors. It misclassifies two CNV images as Other and twenty-two Other images as CNV. The matrices also show the classifiers can classify Normal and DME class images accurately.

Fig. 10 shows two confusion matrices of the proposed deep learning methods. Fig. 10(a) is for Model 1 and Fig. 10(b) is for Model 2. As shown in both matrices, CNV, DME, and Normal class images are labeled accurately with minor error. However, most major errors occur in the Drusen class. Twelve and ten Drusen class images are labeled as CNV in Model 1 and Model 2, respectively.

Table V shows the comparison of the proposed methods with other existing deep learning methods. We focus on comparing the results between multiple binary classifiers and a multi-class classifier. Among the methods, the method using ResNet101 [18] and our proposed methods use multiple binary classifiers. The remaining methods use one or more multi-class classifiers. Our proposed models shows good performance compared to the other methods. Especially, when comparing multi-class classifiers using DenseNet101 [10], InceptionV3 [12], and ResNet152 [14], the proposed method (Model 2) shows better performance. It shows that the proposed two models show relatively better performance than models using a single multi-class CNN classifier.

TABLE III. ACCURACY OF THE PROPOSED MODEL 1 USING THREE BINARY CLASSIFIERS

Classifier- (Normal Drusen) VS. (CNV & DME) (Classifier 1)	**Classifier-** (CNV vs. DME) (Classifier 2)	**Classifier-** (Drusen vs. Normal) (Classifier 3)	**Accuracy**
VGG16	VGG16	VGG16	0.964
VGG19	VGG19	VGG19	0.970
ResNet50	ResNet50	ResNet50	0.969
ResNet152	ResNet152	ResNet152	0.966
DenseNet201	DenseNet201	DenseNet201	0.972
InceptionV3	InceptionV3	InceptionV3	**0.977**
ResNet152	**InceptionV3**	**VGG19**	**0.981**

TABLE IV. ACCURACY OF THE PROPOSED MODEL 2 USING FOUR BINARY CLASSIFIERS

Classifier-CNV (Classifier 1)	**Classifier-DME** (Classifier 2)	**Classifier-Drusen** (Classifier 3)	**Classifier-Normal** (Classifier 4)	**Accuracy**
VGG16	VGG16	VGG16	VGG16	0.975
VGG19	VGG19	VGG19	VGG19	**0.978**
ResNet50	ResNet50	ResNet50	ResNet50	0.972
ResNet152	ResNet152	ResNet152	ResNet152	0.972
DenseNet201	DenseNet201	DenseNet201	DenseNet201	0.968
InceptionV3	InceptionV3	InceptionV3	InceptionV3	0.972
VGG16	**VGG16**	**VGG19**	**InceptionV3**	**0.987**

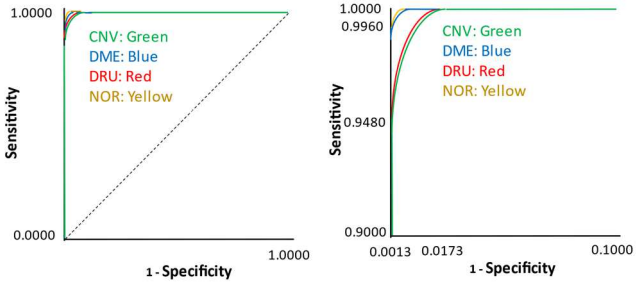

Figure 7. ROC curves of the four binary CNN classifiers used in the proposed deep learning model (Model 2). The left figure shows ROC curves and the right figure shows the curves zoomed in the top left corner of the ROC curves.

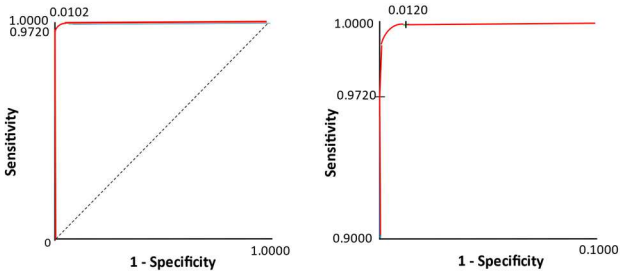

Figure 8. ROC curves of the proposed deep learning model (Model 2) using the four CNN classifiers. The left figure shows ROC curves and the right figure shows the curves zoomed in the top left corner of the ROC curves.

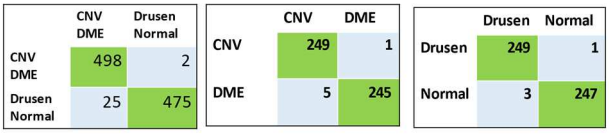

(a)

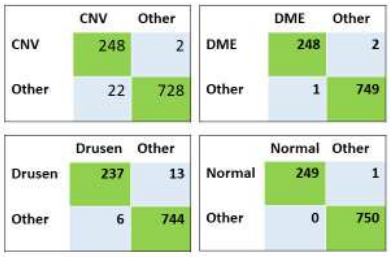

(b)

Figure 9. Confusion matrices of the binary CNN classifiers used in the proposed two deep learning models. (a) Model 1. (b) Model 2.

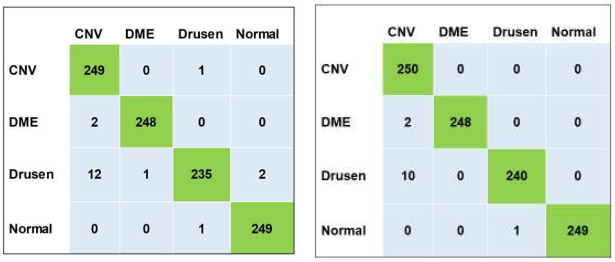

(a) (b)

Figure 10. Confusion matrices of the proposed deep learning models. (a) Model 1. (b) Model 2.

TABLE V. PERFORMANCE COMPARISION OF THE PROPOSED METHODS WITH OTHER DEEPL LEARNING ALGORITHMS

Method	CNN Type	CNNs	Acc.	Sen.	Spec.
Islam et al. [10]	Multi Class	DenseNet101	0.986	-	0.995
Kermany et al. [12]	Multi Class	Inception V3	0.966	0.978	0.974
Kim et al. [14]	Multi Class	ResNet152	0.981	0.981	0.994
Li et al. [15]	Multi Class	ResNet50	0.979	0.968	0.994
Lu et al. [18]	Binary Class	ResNet101	0.959	0.942	0.964
Proposed Method 1	Binary Class	ResNet152, VGG19, InceptionV3	**0.981**	**0.981**	**0.994**
Proposed Method 2	Binary Class	VGG16, VGG19, InceptionV3	**0.987**	**0.987**	**0.996**

IV. CONCLUSIONS

This paper proposes deep learning models to categorize OCT images into four classes using binary CNN classifiers. Preprocessing algorithms are used to remove noise in the images using a FCN and to crop retina layers from the images. Binary CNN classifiers are adapted using six different pre-trained CNN models as feature extractors to make classifiers for CNV, DME, Drusen, and Normal classes. The proposed models multiply the outputs of the three or four binary CNN classifiers to estimate the final outputs. Among them, the model using VGG16 for Classifier-CNV, VGG16 for Classifier-DME, VGG19 for Classifier-Drusen, and InceptionV3 for Classifier-Normal shows the best performance with 0.9870 accuracy, 0.987 sensitivity, and 0.996 specificity. Among the four binary classifiers, Classifier-Normal has the best performance with 0.999 accuracy. These results prove that the multiple binary classifiers can have better performance than multi-class classifiers. It also shows their potential to work as a second reader for ophthalmologists when screening abnormalities among OCT images. In future work, we plan to further investigate new architectures of the deep learning model and handcrafted features to improve classification accuracy.

ACKNOWLEDGMENT

This research was carried out by staff of the National Library of Medicine (NLM), National Institutes of Health, with support from NLM. We thank Lan Le for generating annotation images to segment retina layers in OCT images.

REFERENCES

[1] Americal Academy of Ophthalmology, https://www.aao.org/eye-health/treatments/what-is-optical-coherence-tomography

[2] S. Aumann, S. Donner, J. Fischer, and F. Müller, High Resolution Imaging in Microscopy and Ophthalmology: New Frontiers in Biomedical Optics, Springer, August, 2019

[3] Age-Related Macular Degeneration, https://www.nei.nih.gov/learn-about-eye-health/eye-conditions-and-diseases/age-related-macular-degeneration.

[4] Age-related macular degeneration, NICE Guideline, No. 82, National Institute for Health and Care Excellence (UK), January, 2018.

[5] American Macular Degeneration Foundation, https://www.macular.org/dry-vs-wet-macular-degeneration.

[6] M R Kesen and S W Cousins, Choroidal Neovascularization, Encyclopedia of the Eye, Elsevier Ltd., pp. 257-265, 2010.

[7] https://aerpio.com/therapeutic-areas/wet-amddme/

[8] S.R. Cohen and T.W. Gardner, "Diabetic Retinopathy and Diabetic Macular Edema", Dev Ophthalmology, Vol 55, pp. 137-146, 2016

[9] G. Huang, Z Liu, L.V.D. Maaten, K.Q. Weinberger, "Densely Connected Convolutional Networks", CVPR 2017.

[10] K.T. Islam, S. Wijewickrema, and S. O'Leary, "Identifying Diabetic Retinopathy from OCT Images using Deep Transfer Learning with Artificial Neural Networks", 32nd International Symposium on Computer-Based Medical Systems, pp. 281-286, June 2019.

[11] C. Szegedy, V. Vanhoucke, S. Ioffe, J. Shlens, and Z. Wojna, "Rethinking the Inception Architecture for Computer Vision", IWWW Conference on Cimputer Vision and Pattern Recognition, pp. 2818-2826, 2016.

[12] D.S. Kermany, M. Goldbaum, W. Cai, et al., ''Identifying medical diagnoses and treatable diseases by image-based deep learning,'' Cell, vol. 172, no. 5, pp. 1122–1131, 2018.

[13] K. He, X. Zhang, S. Ren, and J. Sun, "Deep Residual Learning for Image Recognition", IEEE Conference on Computer Vision and Pattern Recognition, pp. 770-778, Las Vegas, USA, 2016.

[14] J. Kim and L. Tran, "Ensemble Learning based on Convolutional Neural Networks for the Classification of Retinal Diseases from Optical Coherence Tomography Images," IEEE 33th International Symposium on Computer-Based Medical Systems, pp 535-540, Rochester, USA, July 2020.

[15] F. Li, H. Chen, Z. Liu, X. Zhang, M. Jiang, Z. Wu, and K. Zhou, "Deep Learning-based Automated Detection of Retinal Diseases Using Ophtical Coherence Tomography Images", Biomedical Optics Express, Vol 10, No 12, pp. 6204-6226, December 2019

[16] K, Simonyan and A. Zisserman, "Very Deep Convolutional Networks for Large-Scale Image Recognition", International Conference on Learning Representations, 2015

[17] F. Li, H. Chen, Z Liu, X. Zhang, and Z. Wu, "Fully Automated Detection of Retinal Disorders by Image Based Deep Learning", Gradfe's Archive for Clinical and Experimental Ophthalmology, 257, pp. 495-505, Jaunary 2019

[18] W. Lu, Y. Tong, Y. Yu, Y. Xing, C. Chen, and Y. Shen, "Depp Learning-Based Automated Classification of Multi-Categorical Abnormalities From Optical Coherence Tomography Images", Translational Vision Science and Technology (TVST), vol. 7, no. 6, pp.1-10, 2018.

[19] ImageNet, http://www.image-net.com.

[20] J. Kim, L. Tran, E. Chew, S. Antani, Optic Disc and Cup Segmentation for Glaucoma Characterization Using Deep Learning, IEEE 32th International Symposium on Computer-Based Medical Systems, pp 489-494, Cordoba, Spain, June 2019

[21] O. Ronneberger, P. Fischer, T. Brox, "U-Net: Convolutional Networks for Biomedical Image Segmentation", Medical Image Computing and Computer-Assisted Intervention (MICCAI), Springer, LNCS, Vol.9351: 234--241, 2015.

[22] https://www.tensorflow.org/

[23] https://keras.io/